

Study on synthesis, crystal structure, antioxidant and DNA-binding of mono-, di- and poly-nuclear lanthanides complexes with bis(*N*-salicylidene)-3-oxapentane-1,5-diamine



Huilu Wu*, Guolong Pan, Yuchen Bai, Yanhui Zhang, Hua Wang, Furong Shi, Xiaoli Wang, Jin Kong

School of Chemical and Biological Engineering, Lanzhou Jiaotong University, Lanzhou 730070, PR China

ARTICLE INFO

Article history:

Received 1 February 2014

Received in revised form 1 April 2014

Accepted 7 April 2014

Available online 18 April 2014

Keywords:

Bis(*N*-salicylidene)-3-oxapentane-1,5-diamine

Lanthanide(III) complex

Crystal structure

DNA-binding property

Antioxidant activity

ABSTRACT

A Schiff base ligand bis(*N*-salicylidene)-3-oxapentane-1,5-diamine **H₂L** have been prepared. Reaction of the shape-specific designed ligand with Ln(NO₃)₃·6H₂O afforded three novel complexes, namely, Sm(**L**)(NO₃)(DMF)(H₂O) **1**, [Eu(**H₂L**)₂(NO₃)₃]_n **2** and Tb₂(**L**)₂(NO₃)₂ **3**. The ligand and complexes were characterized by elemental analysis, UV-Vis, IR, NMR spectroscopy and X-ray crystallography. It is noteworthy that the complexes demonstrate three different types of the structure which changed according to the charge density and acidity of the lanthanide. Complex **1** is a discrete mononuclear species that Sm(III) ion is nine-coordinated in the structure and forming a distorted tricapped trigonal prism geometry. Complex **2** is possessed a 1-D ribbon framework constructed from an extended array of ten-coordinated Eu³⁺ centers and the Schiff base ligands. Complex **3** is revealed as a centrosymmetric binuclear neutral entity, in which Tb(III) ion is eight-coordinated with the coordination surround of distorted square antiprism geometry. In order to explore the relationship between the structure and biological properties, the DNA-binding properties have been investigated by electronic absorption, fluorescence, and viscosity measurements. The results suggest that the ligand and complexes bind to DNA *via* groove modes. The intrinsic binding constants *K_b* of the complexes **1–3** are $(1.19 \pm 0.112) \times 10^5$, $(4.22 \pm 0.086) \times 10^4$ and $(3.89 \pm 0.104) \times 10^4 \text{ M}^{-1}$ respectively. Moreover, the antioxidant activity experiments show that these compounds also exhibit good antioxidant activities against OH[•] and O₂^{•-} *in vitro* studies.

© 2014 Elsevier B.V. All rights reserved.

1. Introduction

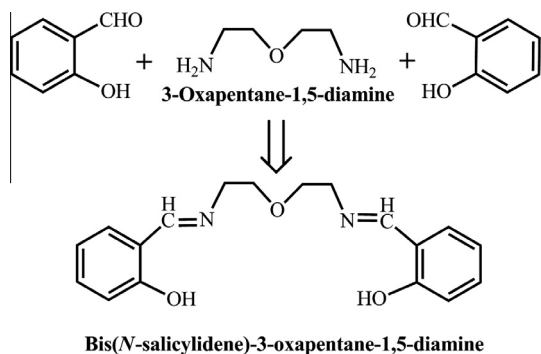
Studies on the synthesis and DNA-binding property of metal complexes are currently receiving much attention due to their various uses in nucleic acid chemistry, especially their potential applications in DNA molecule probes and chemotherapeutic reagents [1–3]. Especially, the relevance and importance of this kind of organic [4,5] and inorganic complex [6–8] molecules intensified extensive research in drug discovery, including cancer chemotherapy. Basically, the complex bound to DNA through three non-covalent modes: intercalation, groove binding and external static electronic effects [9–11]. Therefore, an understanding of how these small molecules bind to DNA will potentially be useful in the design of such new compounds, which can recognize specific sites or conformations of DNA [12,13].

In recent years, the rational design and synthesis of lanthanide coordination complexes have attracted great interest for their

fascinating architectures and potential application as functional materials [14–16]. Particularly, biological activity and also number of other applications resulted in strongly increasing interest for lanthanides [17,18]. One of the most studied applications is usage of the lanthanide molecule complexes to address DNA/RNA by non-covalent binding and/or cleavage [19–21]. In addition, the interest in the chelation of metal ions by Schiff base macrocyclic (coronands) and open-chain (podands) ligands has continually increased owing to the recognition of the role of played by these structures in bioinorganic and medicinal inorganic chemistry [22,23]. So, well designed organic ligands enable a fine tuning of special properties of the metal ions. The lanthanide ions are oxophilic. They are expected to interact strongly with polarised oxygen-bearing functional groups such as salicylide groups [24,25]. Herein, we introduce the synthesis and structural characterization of lanthanide complexes with the Schiff base ligand bis(*N*-salicylidene)-3-oxapentane-1,5-diamine (Scheme 1). The pentadentate ligand contains strong donors, namely phenoxo oxygen atoms as well as imine nitrogen atoms bearing an excellent coordination ability with metal ions through its N₂O₃ donor set.

* Corresponding author. Tel.: +86 13893117544.

E-mail address: wuhuilu@163.com (H. Wu).



Scheme 1. Schematic diagram showing the synthesis of ligand **H₂L**.

On the other hand, an excess of activated oxygen species in the forms of superoxide anion ($O_2^{\cdot-}$) and hydroxyl radical (OH^{\cdot}), generated by normal metabolic processes, may cause various diseases such as carcinogenesis, drug-associated toxicity, inflammation, atherogenesis, and aging in aerobic organisms [26]. Although a variety of (OH^{\cdot}) scavengers are known, their application is limited by: (1) the requirement of unphysiologically high scavenger concentrations which depend on the rate constant, (2) toxic side effects including initiation of further radical chain reactions, or (3) the instability of the compound in biological systems [27]. Many researchers have been working hard to develop complexes in order to achieve the efficient scavenger. It has been recently demonstrated that some minor groove binders for DNA are effective inhibitors of the formation of a DNA/TBP complex or topoisomerases [28,29]. In this paper, we give a full account of the synthesis, crystal structure, DNA-binding properties and antioxidant activities of three Ln(III) complexes with bis(*N*-salicylidene)-3-oxapentane-1,5-diamine.

2. Experimental

2.1. Materials and measurements

All chemicals were of analytical grade. Calf thymus DNA (CT-DNA), ethidium bromide (EB), nitroblue tetrazolium nitrate (NBT), methionine (MET) and riboflavin (VitB₂) were obtained from Sigma-Aldrich Co. (USA) and used without purification. The solution of CT-DNA gave a ratio of UV absorbance at 260 and 280 nm, A_{260}/A_{280} , of 1.8–1.9, indicating that the DNA was sufficiently free of protein [30]. The stock solution of DNA (2.5×10^{-3} M) was prepared in 5 mM Tris-HCl/50 mM NaCl buffer solution (pH = 7.2, stored at 4 °C and used when not more than 4 days). The CT-DNA concentration per nucleotide was determined spectrophotometrically by employing an extinction coefficient of $6600 \text{ M}^{-1} \text{ cm}^{-1}$ at 260 nm [31]. The stock solution of complex was dissolved in DMF at the concentration 3×10^{-3} M.

The C, H and N elemental analyses were determined using a Carlo Erba 1106 elemental analyzer. IR spectra were recorded from 4000 to 400 cm^{-1} with a Nicolet FT-VERTEX 70 spectrometer using KBr pellets. Electronic spectra were taken on Lab-Tech UV Bluestar and Spectrumlab 722sp spectrophotometers and the spectral resolution used is 0.2 nm. Fluorescence spectra were recorded on a LS-45 spectrofluorophotometer. ^1H NMR spectra were obtained with a Mercury plus 400 MHz NMR spectrometer with TMS as internal standard and CDCl_3 as solvent.

2.2. Synthesis

2.2.1. Synthesis of 3-oxapentane-1,5-diamine

3-Oxapentane-1,5-diamine was synthesized following the procedure in Ref. [32]. Found (%): C, 45.98; H, 11.50; N, 26.76. Calcd.

(%) for $\text{C}_4\text{H}_{12}\text{N}_2\text{O}$: C, 46.25; H, 11.54; N, 26.90. FT-IR (KBr ν/cm^{-1}): 1120, $\nu(\text{C}-\text{O}-\text{C})$; 3340, $\nu(-\text{NH}_2)$ stretching frequency, respectively.

2.2.2. Synthesis of **H₂L**

For the synthesis of **H₂L**, salicylic aldehyde (10 mmol, 1.22 g) in EtOH (5 mL) was added dropwise to a 5 mL EtOH solution of 3-oxapentane-1,5-diamine (5 mmol, 0.52 g). After the completion of addition, the solution was stirred for an additional 4 h at 78 °C. After cooling to room temperature, the precipitate was filtered. The product was dried in *vacuo*, and obtained yellow crystalline solid. Yied: 1.19 g (68.5%). Found (%): C, 69.09; H, 6.54; N, 8.83. Calcd. (%) for $\text{C}_{18}\text{H}_{20}\text{O}_3\text{N}_2$: C, 69.21; H, 6.45; N, 8.97. ^1H NMR (CDCl_3 400 MHz) δ/ppm : 8.30 (s, 2H, $\text{N}=\text{C}-\text{H}$), 6.79–7.33 (m, 8H, H-benzene ring), 3.66–3.74 (m, 8H, $\text{O}-(\text{CH}_2)_2-\text{N}=\text{C}$). UV-Vis (λ , nm): 268, 316. FT-IR (KBr ν/cm^{-1}): 1637, $\nu(\text{C}=\text{N})$; 1286, $\nu(\text{C}-\text{O}-\text{C})$; 3458, $\nu(\text{OH})$ stretching frequency, respectively.

2.2.3. Preparation of complexes

Three complexes were prepared by a similar procedure. To a stirred solution of **H₂L** (156 mg, 0.5 mmol) in EtOH (10 mL) was added $\text{Ln}(\text{NO}_3)_3(\text{H}_2\text{O})_6$ (0.5 mmol; Sm, 222 mg; Eu, 223 mg; Tb, 226 mg) and triethylamine (0.3 mL) in EtOH (10 mL). The yellow sediment generated rapidly. The precipitate was filtered off, washed with EtOH and absolute Et₂O, and dried in *vacuo*. The dried precipitate was dissolved in DMF to form a yellow solution. The yellow block crystals of the Ln(III) complexes that suitable for X-ray diffraction studies were obtained by vapor diffusion of diethyl ether into the solution for few weeks at room temperature.

$\text{Sm}(\text{L})(\text{NO}_3)(\text{DMF})(\text{H}_2\text{O})$ **1**. Yield: 224 mg, 59.3%. Found (%): C, 40.82; H, 4.71; N, 8.88. Calcd. (%) for $\text{C}_{21}\text{H}_{27}\text{N}_4\text{O}_8\text{Sm}$: C, 41.09; H, 4.43; N, 9.13. UV-Vis (λ , nm): 268, 316. FT-IR (KBr ν/cm^{-1}): 1290, $\nu(\text{C}-\text{O}-\text{C})$; 1362, 1031, $\nu(\text{NO}_3)$; 1632, $\nu(\text{C}=\text{N})$ stretching frequency, respectively.

$[\text{Eu}(\text{H}_2\text{L})_2(\text{NO}_3)_3]_n$ **2**. Yield: 186 mg, 49.1%. Found (%): C, 44.58; H, 4.41; N, 9.97. Calcd. (%) for $\text{C}_{36}\text{H}_{40}\text{EuN}_7\text{O}_{15}$: C, 44.91; H, 4.19; N, 10.18. UV-Vis (λ , nm): 269, 316. FT-IR (KBr ν/cm^{-1}): 1292, $\nu(\text{C}-\text{O}-\text{C})$; 1365, 1051, $\nu(\text{NO}_3)$; 1633, $\nu(\text{C}=\text{N})$ stretching frequency, respectively.

$\text{Tb}_2(\text{L})_2(\text{NO}_3)_2$ **3**. Yield: 199 mg, 52.1%. Found (%): C, 40.30; H, 3.73; N, 7.56. Calcd. (%) for $\text{C}_{36}\text{H}_{40}\text{N}_6\text{O}_{14}\text{Tb}_2$: C, 40.69; H, 3.41; N, 7.91. UV-Vis (λ , nm): 269, 316. FT-IR (KBr ν/cm^{-1}): 1214, $\nu(\text{C}-\text{O}-\text{C})$; 1368, 1052, $\nu(\text{NO}_3)$; 1633, $\nu(\text{C}=\text{N})$ stretching frequency, respectively.

2.3. X-ray crystallography

A suitable single crystal was mounted on a glass fiber, and the intensity data were collected on a Bruker Smart CCD diffractometer with graphite-monochromated Mo $K\alpha$ radiation ($\lambda = 0.71073 \text{ \AA}$) at 296 K. Data reduction and cell refinement were performed using the SMART and SAINT programs. The absorption corrections are carried out by the empirical method [33]. The structure was solved by direct methods and refined by full-matrix least-squares against F^2 of data using SHELXTL software [34]. The uncoordinated water molecule was found to be disordered. Its electron density was removed from the reflection intensities by using the routine SQUEEZE in PLATON. All H atoms were found in difference electron maps and subsequently refined in a riding-model approximation with C–H distances ranging from 0.93 to 0.97 Å and $U_{\text{iso}}(\text{H}) = 1.2 U_{\text{eq}}(\text{C})$ or $1.5 U_{\text{eq}}(\text{C})$. The crystal data and experimental parameters relevant to the structure determination are listed in Table 1. Selected bond lengths and angles are presented in Table S1.

Table 1
Crystal and structure refinement data for complexes **1**, **2** and **3**.

Complex	1	2	3
Empirical formula	C ₂₁ H ₂₇ N ₄ O ₈ Sm	C ₃₆ H ₄₀ EuN ₇ O ₁₅	C ₃₆ H ₃₆ N ₆ O ₁₂ Tb ₂
Molecular weight	613.82	962.71	1062.55
Crystal system	Monoclinic	Monoclinic	Monoclinic
Space group	P2(1)/n	C2/c	C2/c
a (Å)	11.564(7)	14.052(7)	29.224(20)
b (Å)	11.973(7)	16.276(8)	11.766(8)
c (Å)	18.496(11)	17.397(9)	15.117(10)
α (°)	90	90	90
β (°)	106.471(6)	102.038(6)	117.552(7)
γ (°)	90	90	90
V (Å ³)	2456(2)	3891(3)	4608(5)
Z, Dc (mg/m ³)	4	4	4
μ (mm ⁻¹)	2.443	1.692	3.103
F(000)	1228	1952	2080
θ Range for data collection(°)	2.30–25.49	2.39–25.50	2.65–25.50
Crystal size (mm)	0.25 × 0.23 × 0.20	0.28 × 0.25 × 0.22	0.26 × 0.24 × 0.21
Limiting indices, h k l	–14 to 13 –11 to 14 –22 to 22	–9 to 16 –14 to 19 –21 to 21	–35 to 33 –13 to 14 –18 to 18
Reflections collected	12,959	8886	12,187
Unique reflections	4541	3595	4255
R _{int}	0.0533	0.0641	0.0487
Data/restraints/parameters	4541/3/309	3595/0/268	4255/0/253
Goodness-of-fit on F ²	1.006	1.008	0.927
R ₁ /wR ₂ [I > 2σ(I)]	0.0331/0.0611	0.0506/0.0819	0.0399/0.0932
R ₁ /wR ₂ (all data)	0.0534/0.0672	0.0699/0.0881	0.0665/0.1015
Largest diff. peak, hole (e Å ⁻³)	0.562, –0.848	1.003, –0.765	1.426, –1.547

2.4. DNA-binding study methods

2.4.1. Electronic absorption titration

All spectrophotometric measurements were performed in thermostated quartz sample cells at 25 °C. Solutions for analysis were prepared by dilution of stock solutions immediately before the experiments. Spectrophotometer slit widths were kept at 1 nm for absorption spectroscopy and 5/5 nm for emission spectroscopy. Electronic absorption titration experiments were performed by maintaining the concentration of the test compounds (ligand/complexes) as constant (30 μM) while gradually increasing the concentration of CT-DNA. To obtain the absorption spectra, the required amount of CT-DNA was added to both compound solution and the reference solution to eliminate the absorbance of CT-DNA itself [35,36]. Each sample solution was scanned in the range of 190–500 nm, and the mixture was allowed to equilibrate for 5 min before the spectra were recorded. From the absorption titration data, the binding constant (K_b) was determined using the equation [9,10]:

$$[\text{DNA}]/(\varepsilon_a - \varepsilon_f) = [\text{DNA}]/(\varepsilon_b - \varepsilon_f) + 1/K_b(\varepsilon_b - \varepsilon_f)$$

where [DNA] is the concentration of CT-DNA in base pairs, ε_a corresponds to the extinction coefficient observed (Aobsd/[M]), ε_f corresponds to the extinction coefficient of the free compound, ε_b is the extinction coefficient of the compound when fully bound to CT-DNA, and K_b is the intrinsic binding constant. The ratio of slope to intercept in the plot of [DNA]/($\varepsilon_a - \varepsilon_f$) versus [DNA] gave the value of K_b .

2.4.2. Fluorescence studies

EB emits intense fluorescence in the presence of CT-DNA, due to its strong intercalation between the adjacent CT-DNA base pairs. It was previously reported that the enhanced fluorescence can be quenched by the addition of a second molecule [37]. The extent of fluorescence quenching of EB bound to CT-DNA can be used to determine the extent of binding between the second molecule and CT-DNA. The effect of each complex with the DNA–EB complex was

studied by adding a certain amount of a solution of the complex step by step into the buffer solution of the DNA–EB complex [38]. The fluorescence spectra of EB were measured using an excitation wavelength of 520 nm, and the emission range was set between 550 and 750 nm. The influence of the addition of each compound to the DNA–EB complex solution has been obtained by recording the variation of the fluorescence emission spectra. The spectra were analyzed according to the classical Stern–Volmer equation [39]:

$$I_0/I = 1 + K_{sv}[Q] = 1 + K_q\tau_0[Q]$$

where I_0 and I are the fluorescence intensities at 599 nm in the absence and presence of the quencher, respectively, K_{sv} is the linear Stern–Volmer quenching constant, [Q] is the concentration of the quencher, K_q is the quenching rate constant and τ_0 is luminescence decay time in absence of the quencher. In these experiments [CT-DNA] = 2.5×10^{-3} mol/L, [EB] = 2.2×10^{-3} mol/L.

2.4.3. Viscosity titration measurements

Viscosity experiments were conducted on an Ubbelodhe viscometer, immersed in a water bath maintained at 25.0 ± 0.1 °C. The flow time was measured with a digital stopwatch and each sample was tested, three times to get an average calculated time. Titrations were performed for the complexes (3–30 μM), and each compound was introduced into CT-DNA solution (42.5 μM) present in the viscometer. Data were analyzed as $(\eta/\eta_0)^{1/3}$ versus the ratio of the concentration of the compound to CT-DNA, where η is the viscosity of CT-DNA in the presence of the compound and η_0 is the viscosity of CT-DNA alone. Viscosity values were calculated from the observed flow time of CT-DNA-containing solutions corrected from the flow time of the 5 mM Tris-HCl/50 mM NaCl buffer alone (t_0), $\eta = (t - t_0)$ [40].

2.5. Antioxidation study methods

2.5.1. Hydroxyl radical assay

Hydroxyl radicals were generated in aqueous media through the Fenton-type reaction [41]. The aliquots of reaction mixture

(3 mL) contained 1 mL of 0.1 mmol aqueous safranin, 1 mL of 1.0 mmol aqueous EDTA-Fe(II), 1 mL of 3% aqueous H₂O₂, and a series of quantitative microadditions of solutions of the test compound. A sample without the tested compound was used as the control. The reaction mixtures were incubated at 37 °C for 30 min in a water bath. The absorbance was then measured at 520 nm. All the tests were run in triplicate and are expressed as the mean and standard deviation (SD) [42]. The scavenging effect for OH[•] was calculated from the following expression:

$$\text{Scavenging ratio (\%)} = [(A_i - A_0)/(A_c - A_0)] \times 100\%$$

where A_i = absorbance in the presence of the test compound; A_0 = absorbance of the blank in the absence of the test compound; A_c = absorbance in the absence of the test compound, EDTA-Fe(II) and H₂O₂.

2.5.2. Superoxide radical assay

A nonenzymatic system containing 1 mL 9.9 × 10⁻⁶ M VitB₂, 1 mL 1.38 × 10⁻⁴ M NBT, 1 mL 0.03 M MET were used to produce superoxide anion (O₂^{•-}), and the scavenging rate of O₂^{•-} under the influence of 0.1–1.0 μM tested compound was determined by monitoring the reduction in rate of transformation of NBT to monoformazan dye [43]. The solution of MET, VitB₂ and NBT were prepared with 0.02 M phosphate buffer (pH = 7.8) at the condition of avoiding light. The reactions were monitored at 560 nm with a UV-Vis spectrophotometer, and the rate of absorption change was determined. The percentage inhibition of NBT reduction was calculated using the following equation [44]: percentage inhibition of NBT reduction = (1 - k'/k) × 100, where k' and k present the slopes of the straight line of absorbance values as a function of time in the presence and absence of SOD mimic compound (SOD is superoxide dismutase), respectively. The IC₅₀ values for the complexes were determined by plotting the graph of percentage inhibition of NBT reduction against the increase in the concentration of the complex. The concentration of the complex which causes 50% inhibition of NBT reduction is reported as IC₅₀.

3. Results and discussion

The Ln(III) complexes were prepared by reaction of **H₂L** with Ln(NO₃)₃(H₂O)₆ in ethanol. They are soluble in polar aprotic solvents such as DMF, DMSO and MeCN, slightly soluble in water, ethanol, methanol, ethyl acetate, and chloroform and insoluble in Et₂O and petroleum ether. The elemental analysis shows that their composition which were confirmed by the crystal structure analysis.

3.1. IR and electronic spectra

The IR spectra of the Ln(III) complexes (Ln = Sm, Eu and Tb) were analyzed in comparison with that of their common free ligand **H₂L** in the region 4000–400 cm⁻¹. In the free ligand **H₂L**, a strong band is found at 1637 cm⁻¹ together along with a weak band at 1286 cm⁻¹. By analogy with the assigned bands, the former can be attributed to ν(C=N), while the latter can be attributed to ν(C–O–C) [45,46]. The location of the two bands was slightly shifted for complex **1**, the band at 1637 cm⁻¹ is shifted to 1632 cm⁻¹ and the band at 1286 cm⁻¹ is shifted to 1290 cm⁻¹, which can be attributed to the coordination of the ligand to the metal center atom. Similar shifts also appear in complexes **2** (1633, 1292 cm⁻¹) and **3** (1633, 1214 cm⁻¹), which gives the same conclusion. Moreover, bands at 1362, 1031 cm⁻¹ in **1**, 1365, 1051 cm⁻¹ in **2** and 1368, 1052 cm⁻¹ in **3** indicate that nitrate is bidentate [47], in agreement with X-ray diffraction.

DMF solutions of the ligand **H₂L** and Ln(III) complexes show, as expected, almost identical UV spectra. The UV bands of **H₂L** (268,

316 nm) are marginally shifted in complexes, which provide clear evidence for nitrogen and oxygen atom coordination to metal ions. Two absorption bands are assigned to π → π* (benzene) and π → π* (C=N) transitions [48].

3.2. X-ray structures of the complexes

The crystal analysis unambiguously reveals that complex **1** crystallizes in monoclinic space group *P2(1)/n*. The crystal structure of Sm(L)(NO₃)(DMF)(H₂O) demonstrates a discrete mononuclear species with the Sm(III) center in a nine-coordinate SmN₂O₇ coordination geometry [two imine N–N(1), N(2) from the amine part; one ether O–O(1); two coordinated phenoxo O–O(2) and O–O(3); one O–O(4) from DMF; two O–O(6) and O(7) from bidentate univalent NO₃⁻ and one coordinated water O–O(5)] as shown in Fig. 1(a). The coordination polyhedron around Sm(III) is a distorted tricapped trigonal prism (Fig. 1(b)). The bond lengths are in the range Sm–O_{phenoxo}: 2.303(3)–2.333(3), Sm–O_{ether}: 2.619(3), Sm–O_{DMF}: 2.448(3), Sm–O_{nitrate}: 2.550(3)–2.598(3) and Sm–O_{water}: 2.439(3) Å, all of which are within the range of those observed for other nine-coordinated Ln(III) complexes with oxygen donor ligands [49,50].

Hydrogen-bonding interactions play important roles in crystal packing of **1** [51]. As shown in Fig. 2, the neighboring [Sm(L)(NO₃)(DMF)(H₂O)] moieties are connected by two hydrogen bonds between the metal-coordinated H₂O and the ligand with O(5)··O(2) and O(5)··O(3) distances of 2.713(4) Å and 2.740(4) Å and an infinite 2-D (two dimension) layer is propagated due to the Hydrogen-bonding interactions. Moreover, each molecule is linked by hydrogen bonds between the coordinated ligands to form an infinite 3-D network (Fig. S1). The distinct topological structure affords an opportunity to investigate the potential in molecular recognition and gas absorption.

The single-crystal X-ray analysis reveals that complex **2** crystallizes in monoclinic space group *C2/c* and possesses a 1-D ribbon framework constructed from an extended array of ten-coordinated Eu³⁺ centers and the ligands. Each europium ion is coordinated by six oxygen atoms from three bidentate nitrate groups and the other four oxygen atoms from the phenoxo groups of the different ligands, as shown in Fig. 3(a). The coordination polyhedron around Eu(III) is a distorted bicapped square antiprism (Fig. 3(b)). The four ligands act as bridging linkers through their phenoxo oxygen atoms, where Eu–HL–Eu double-stranded helices are found (Fig. S2). Two ligands form an ellipse with two europium ions which are located at the top of the ellipse with the Eu··Eu separation of 12.778 Å, and the two ellipses are linked by the europium ion. The adjacent ellipses are related by a twofold axis which

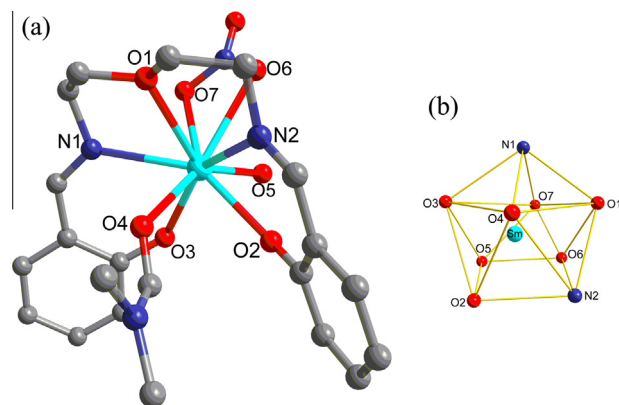


Fig. 1. (a) Ball and stick representation of **1**; H atoms are omitted for clarity. (b) Coordination polyhedron of Sm.

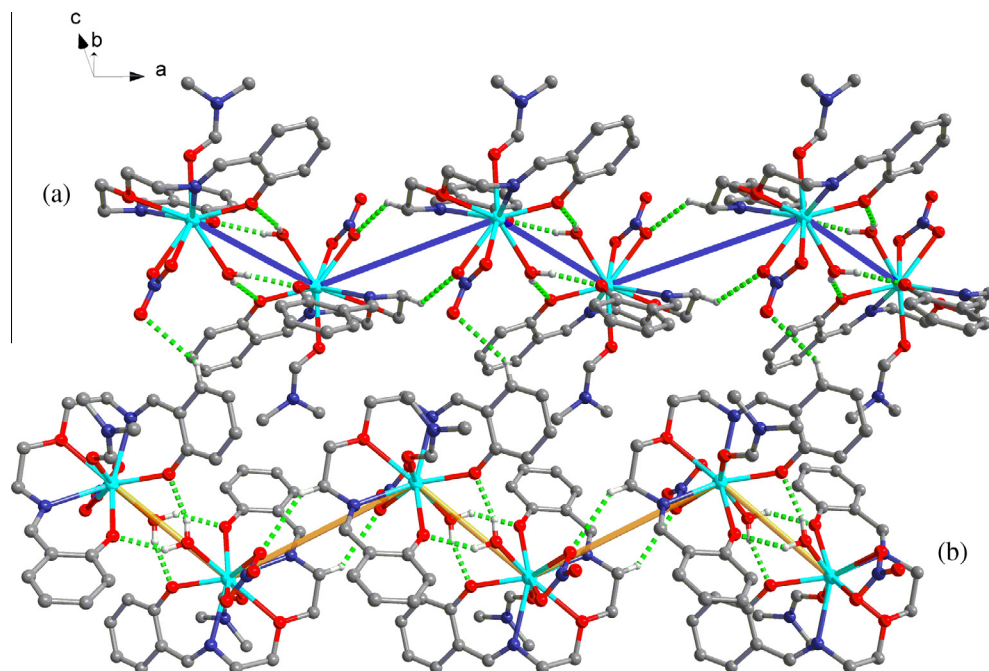


Fig. 2. 2-D layer structure formed of **1** constructed by hydrogen bonding which are indicated with dashed green lines. (For interpretation of the references to color in this figure legend, the reader is referred to the web version of this article.)

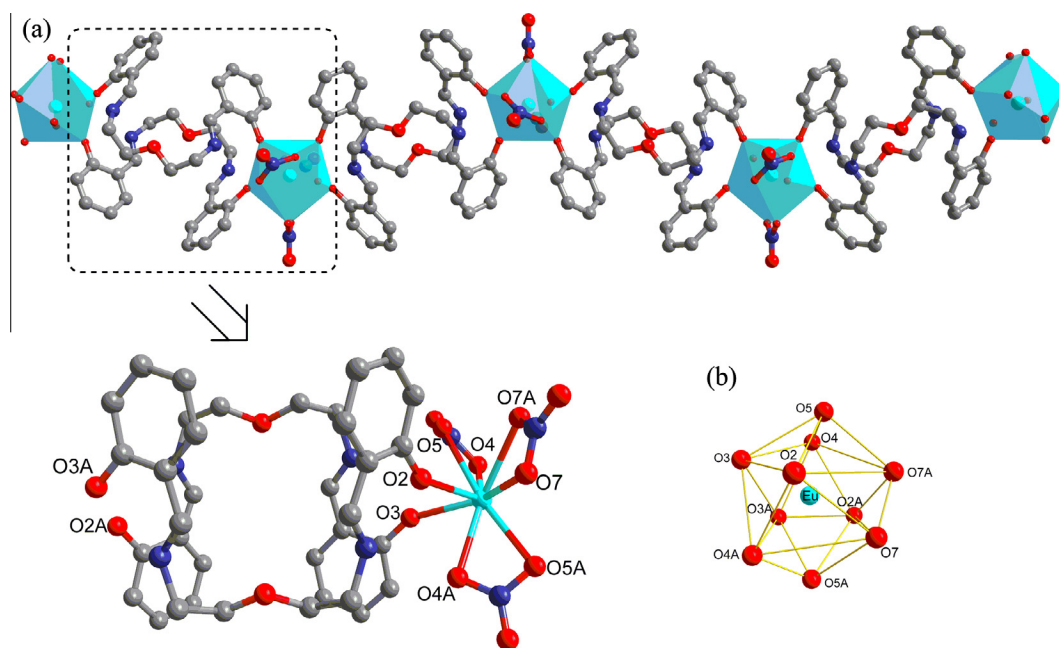


Fig. 3. (a) One-dimensional structure of **2**; H atoms are omitted for clarity. (b) Coordination polyhedron of Eu.

passes through the Eu1 atom and nitro atoms N4, O8. The europium ions in the same chain form an infinite 1D zigzag structure and the $\text{Eu} \cdots \text{Eu} \cdots \text{Eu}$ angle is 147.55° . The chains are packed in the same way, and the adjacent europium atoms in the different chains are in the same plain.

The $\text{Eu}-\text{O}_{\text{phenoxo}}$ distances range from 2.368(4) to 2.373(4) Å and the $\text{Eu}-\text{O}_{\text{nitrate}}$ distances range from 2.549(4) to 2.662(4) Å. The bond length is almost equal to those found in Eu complexes [52,53]. The ligands are disposed in a facial arrangement with $\text{N} \cdots \text{Eu} \cdots \text{N}$ angles being symmetrical, while the $\text{O}(\text{phen-}$

$\text{oxo}) \cdots \text{Eu} \cdots \text{O}(\text{phenoxo})$ in the same ellipse displays a narrower angle of 69.43° . This would appear to be an electrostatic rather than steric effect, with the repulsions from two negatively charged oxygens per nitrate ligand dominating the increased steric repulsions from the bulky phenoxo groups. Most interestingly, the polymer can offer a lot of perfectly cavities to trap guest molecules (Fig. 4). Thus the solid may also have the potential for practical applications such as gas absorption and molecular recognition.

Complex **3** crystallized in the monoclinic space group $C2/c$, and the crystallographic analysis reveals that **3** is a centrosymmetric

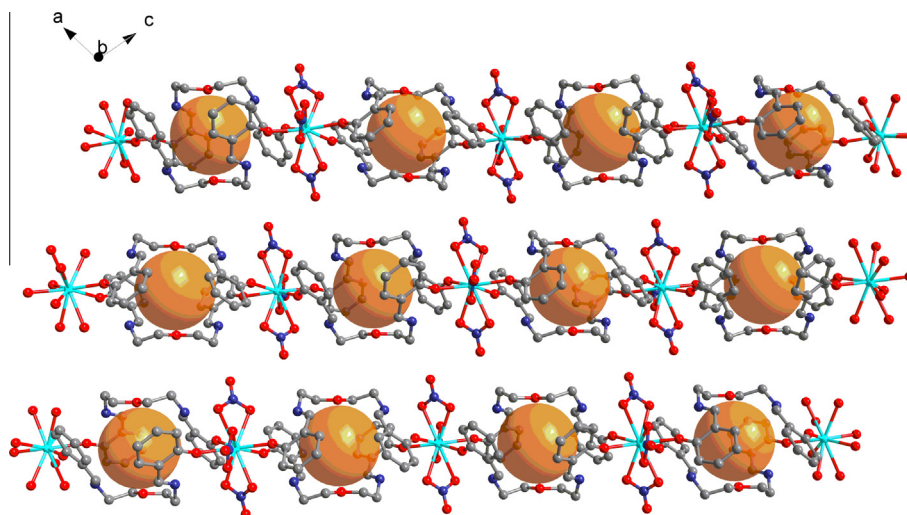


Fig. 4. Parallel arrangement Eu(III) coordination chains contain of cavities, the large orange sphere indicates the size of the cavities. Hydrogen atoms are omitted for clarity.

neutral homobinuclear entity. The structure of **3** (Fig. 5(a)) shows that two adjacent [Tb(L)(NO₃)] moieties are bridged *via* two phenoxo groups. In the μ_2 -diphenoxo bridged binuclear structure both Tb(III) centers are octacoordinated (Fig. 5(b)). The local coordination environment is identical for both the centers by symmetry and is best described as a distorted square TbN₂O₆ antiprism (Fig. 5(b)). Due to the flexibility of the ligand, it loses its planarity. The bond lengths are in the range Tb(1)–N_{imine} 2.495(5)–2.517(6), Tb(1)–O_{ether}: 2.469(4) and Tb(1)–O_{nitrate}: 2.475(4)–2.488(4) Å. The nature of coordination of the two identical Schiff base moieties of the same ligand is completely different. Of the two phenoxo oxygen atoms of each ligand, one is simply monocoordinated while the other one bridges the adjacent Tb(III) centers as reflected by the Tb–O_{phenoxo} bond lengths [Tb(1)–O(2), 2.330(4) and Tb(1)–O(3), 2.181(5) Å]. The distance of Tb(1)–Tb(1A): 3.771(2) Å is relatively too long to consider any direct intramolecular Tb–Tb interaction.

Hydrogen-bonding interactions are also very significant for **3**. The hydrogen bonding interactions lead to the formation of a 2-D supramolecular network as shown in Fig. S3. An interesting feature of this structure is the intermolecular hydrogen bond that exists among the Tb(III) complexes, which also affords approximately $10 \times 8 \text{ \AA}^2$ sized voids to trap guest molecules (Fig. 6). It is worth noting that intermolecular interactions have the potential to assemble smaller and simpler fragments into desired cavities

under favorable conditions, which is important in host–guest chemistry and has applications in chemistry, biology, and materials science.

3.3. DNA binding properties

3.3.1. Absorption spectroscopic studies

Absorption titration can monitor the interaction of a compound with DNA. The obvious hypochromism and red shift are usually characterized by the noncovalently intercalative binding of compounds to DNA helix, due to the strong stacking interaction between the aromatic chromophore of the compound and base pairs of DNA [54]. However, the intercalation between a compound and DNA helix cannot be excluded only by no or small red shift of UV–Vis absorption bands. In fact, some groove binders of Hoechst 33258 family can also present red shifts or even blue shifts of absorption bands when they bind to DNA helix by groove binding modes, especially for multiple binders [55].

To clarify the interactions between the compounds and DNA, the electronic absorption spectra of the ligand and its Ln(III) complexes (Ln = Sm, Eu and Tb) in the absence and in the presence of the CT-DNA (at a constant concentration of the compounds) were obtained, which are shown in Fig. 7, respectively. As can be seen from Fig. 7a–d the ligand and complexes exhibit intense absorption bands at 391–393 nm and addition of increasing amounts of CT-DNA results in hypochromism and bathochromic shift in the UV–Vis spectra of the compounds. In the present case, with addition of DNA, the ligand exhibit hypochromism of about 32.4% accompanied by bathochromism of about a 1–2 nm shift in the absorption maxima. Corresponding complexes exhibit hypochromism of about 70.1%, 68.2% and 58.9%, and also accompanied by bathochromism of about a 1–3 nm shift in the absorption maxima. The hypochromism observed for the $\pi \rightarrow \pi^*$ transition bands indicating strong binding of the compounds to DNA.

To compare quantitatively the affinity of the ligand and Ln(III) complexes towards DNA, the intrinsic binding constants K_b of the two compounds to CT-DNA were determined by monitoring the changes of absorbance with increasing concentration of DNA. The data of intrinsic binding constants K_b are shown in Table 2. The K_b values of the ligand and complexes **1–3** are $(5.30 \pm 0.096) \times 10^3 \text{ M}^{-1}$ ($R^2 = 0.99$ for 16 points), $(1.19 \pm 0.112) \times 10^5 \text{ M}^{-1}$ ($R^2 = 0.99$ for 16 points), $(4.22 \pm 0.086) \times 10^4 \text{ M}^{-1}$ ($R^2 = 0.99$ for 16 points) and $(3.89 \pm 0.104) \times 10^4 \text{ M}^{-1}$ ($R^2 = 0.99$ for 16 points), respectively, from the decay of the absorbances. The K_b values obtained here are lower than that reported for classical intercalator

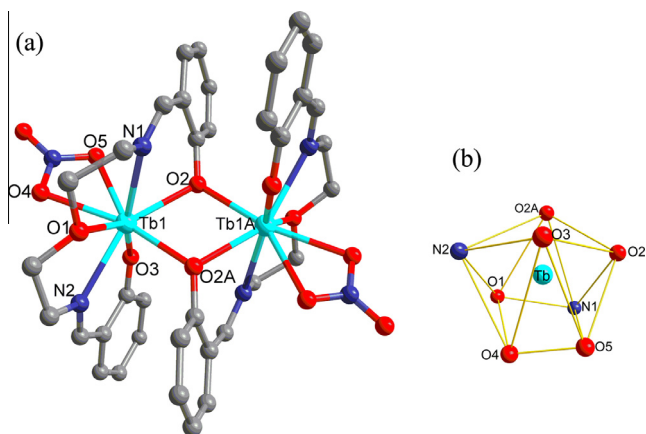


Fig. 5. (a) Ball and stick representation of **3**; H atoms are omitted for clarity. (b) Coordination polyhedron of Tb.

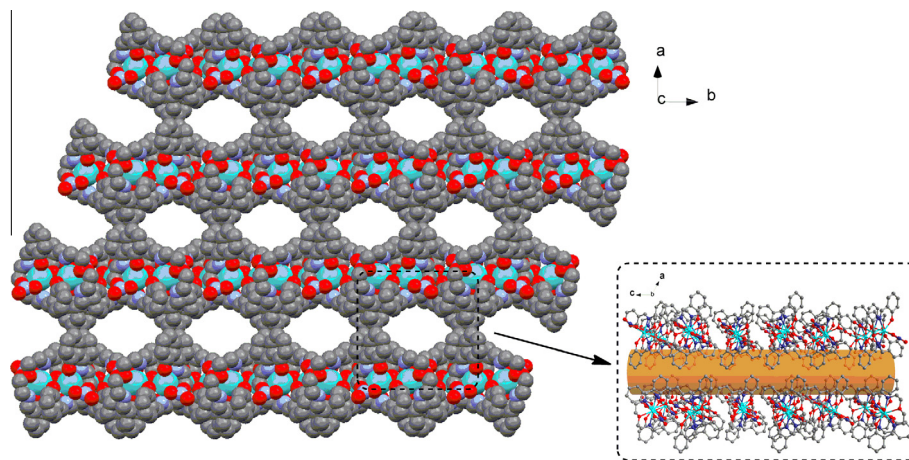


Fig. 6. A space-filling diagram of the nanosized holes in **3**.

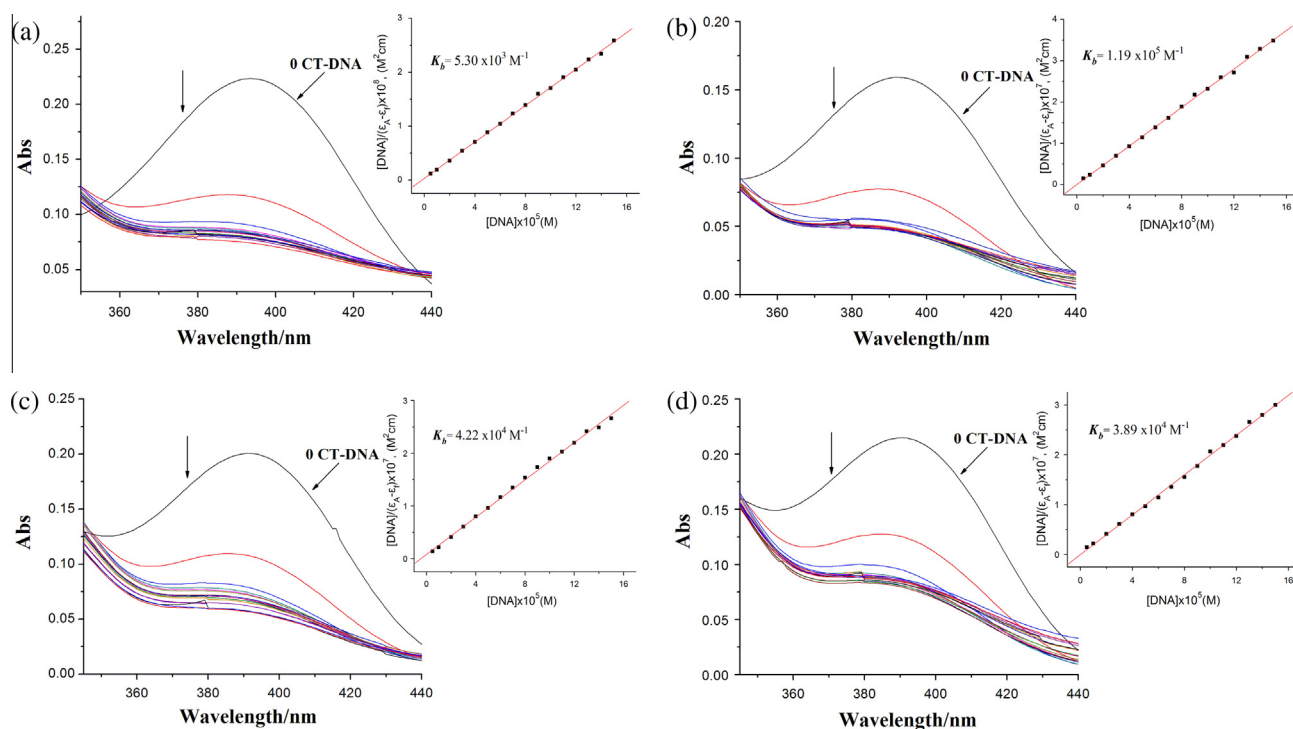


Fig. 7. Absorption spectra of compound **3** in the presence of CT-DNA (the DNA absorption was subtracted). The concentration of the ligand **H₂L** (a) and complexes **1** (b), **2** (c), and **3** (d) was kept constant at $3 \times 10^{-5} \text{ M}^{-1}$. Arrows show the absorbance changes upon increasing DNA concentration. Inset: Plots of $[\text{DNA}]/(\epsilon_a - \epsilon_f)$ versus for the titration of DNA with compound; ■, experimental data points; solid line, linear fitting of the data.

Table 2
Parameters of K_b , K_{SV} and K_q for Ligand and complexes **1**, **2** and **3**.

Compound	$K_b \times 10^5$	$K_{SV} \times 10^4$	K_q
H₂L	0.053 ± 0.0001	0.35 ± 0.010	0.35×10^{12}
1	1.19 ± 0.112	2.01 ± 0.099	2.01×10^{12}
2	4.22 ± 0.086	1.83 ± 0.121	1.83×10^{12}
3	3.89 ± 0.104	1.50 ± 0.075	1.50×10^{12}

(for ethidium bromide and [Ru(phen)DPPZ] whose binding constants have been found to be in the order of 10^6 – 10^7 M^{-1}) [56–58]. It is clear that the hypochromism and K_b values are not enough evidence, but these results can suggest an intimate association of the compounds with CT-DNA and indicate that the binding strength of complex is in the order of $\mathbf{1} > \mathbf{2} > \mathbf{3} > \mathbf{H}_2\mathbf{L}$.

Based on the above results, we found that the affinity for DNA is stronger in case of Ln(III) complexes when compared with the ligand **H₂L**. For this difference, we attributed two possible reasons. (i) The electrostatics of positively charged Ln^{3+} ions cause an interaction with polyanionic DNA. (ii) The charge transfer of coordinated **H₂L**, caused by coordination of the central Ln(III), results in reduction of charge density of the planar conjugated system; this change will lead to complexes binding to DNA more easily [9,10].

3.3.2. Competitive binding with ethidium bromide

The ability of a complex to change the fluorescence intensity of ethidium bromide (EB) in its EB–DNA adduct has been reported as a standard intercalating agent of DNA and it is a reliable tool to measure the affinity of the complex for DNA, irrespective of the binding modes. Therefore, a solution of EB has been used as a

spectral probe since it does not emit in the buffer solution due to probable quenching of its emission by the solvent [59]. However, intense emission is observed when EB strongly intercalates with the adjacent DNA base pairs. But a decrease in emission intensity results from the displacement of EB by a quencher molecule. The extent of emission quenching could be used to determine the extent of binding between the metal complex with DNA [59].

For the ligand H_2L and Ln(III) complexes, no emission was observed either alone or in the presence of CT-DNA in the buffer. The fluorescence quenching of DNA-bound EB by the ligand and complexes **1–3** are shown in Fig. 8a–d. The quenching of EB bound to CT-DNA by the Ln(III) complexes are in good agreement with the linear Stern–Volmer equation, which provides further evidence that the Ln(III) complexes bind to DNA and only one type of quenching process occurs. The data of K_{SV} are presented in Table 2. The K_{SV} values of the ligand H_2L and complexes **1–3** are $(0.35 \pm 0.010) \times 10^4$ ($R^2 = 0.98$ for 21 points in the line part), $(2.01 \pm 0.099) \times 10^4 \text{ M}^{-1}$ ($R^2 = 0.98$ for 10 points), $(1.83 \pm 0.121) \times 10^4 \text{ M}^{-1}$ ($R^2 = 0.98$ for 10 points) and $(1.50 \pm 0.075) \times 10^4 \text{ M}^{-1}$ ($R^2 = 0.98$ for 10 points), respectively. The Stern–Volmer dynamic quenching constants can also be interpreted as binding affinities of the complexation reactions [60]. Consequently, the data of K_{SV} present the order of $\mathbf{1} > \mathbf{2} > \mathbf{3} > \text{H}_2\text{L}$, which is consistent with the previous absorption spectral conclusions. Moreover, the K_q values for the ligand and complexes **1–3** are 0.35×10^{12} , 2.01×10^{12} , 1.83×10^{12} and $1.50 \times 10^{12} \text{ L M}^{-1} \text{ S}^{-1}$, respectively, and were far larger than $2.0 \times 10^{10} \text{ L M}^{-1} \text{ S}^{-1}$, the maximum diffusion collision quenching rate constant of various quenchers with the biopolymer. Consequently, the probable quenching mechanism of fluorescence of the ligand and complexes **1–3** binding reactions should follow a static quenching process rather than a dynamic one [61].

Insert figure in Fig. 8 show the plots of I_0/I versus [Component]. The data of K_{SV} are all at 10^4 M^{-1} level for the ligand and its Ln(III) complexes, accordingly. In view of the strong interaction of EtBr with DNA of which the binding constant of EtBr with DNA is at 10^6 M^{-1}

level [58], we consider it is impossible for the complexes to scramble EtBr from DNA. Similar fluorescence quenching effect of EtBr bound to DNA has been observed for the addition of several groove-binding compounds, including netropsin and distamycin A [21,62]. The observed results make us to suspect that the complexes may interact with DNA through the groove binding mode or intercalation mode, releasing some EtBr molecules from EtBr–DNA system [62–64].

3.3.3. Viscosity titration measurements

Viscosity titration measurements were carried out to further clarify the interaction modes between the investigated compounds and CT-DNA. Hydrodynamic measurements that are sensitive to changes in the length of DNA (i.e. viscosity and sedimentation) are regarded as the least ambiguous and the most critical tests of binding in solution in the absence of crystallographic structural data [65]. The classic intercalation model involves the insertion of a planar molecule between DNA base pairs, which results in a decrease in the DNA helical twist and lengthening of the DNA, the molecule will be in close proximity to the DNA base pairs as well [66]. In contrast, molecule that binds exclusively in the DNA grooves by partial and/or non-classical intercalation, under the same conditions, typically cause less pronounced (positive or negative) or no change in DNA solution viscosity [67].

The effects of the ligand and complexes **1–3** on the viscosity of CT-DNA is shown in Fig. 9. The experimental results exhibited that the addition of the ligand and complexes **1–3** causes no significant viscosity change, indicating that these compounds can bind to DNA by groove modes [67]. In addition, the lanthanide complexes bind to DNA via groove modes, due to the conjugated effect and hydrogen-bonding interactions. It does not alter or destroy DNA conformation and the environment of the complexes [20,21].

3.4. Antioxidant properties

Generation of reactive oxygen species (ROS) is a normal process in the life of aerobic organisms. It has been estimated that free

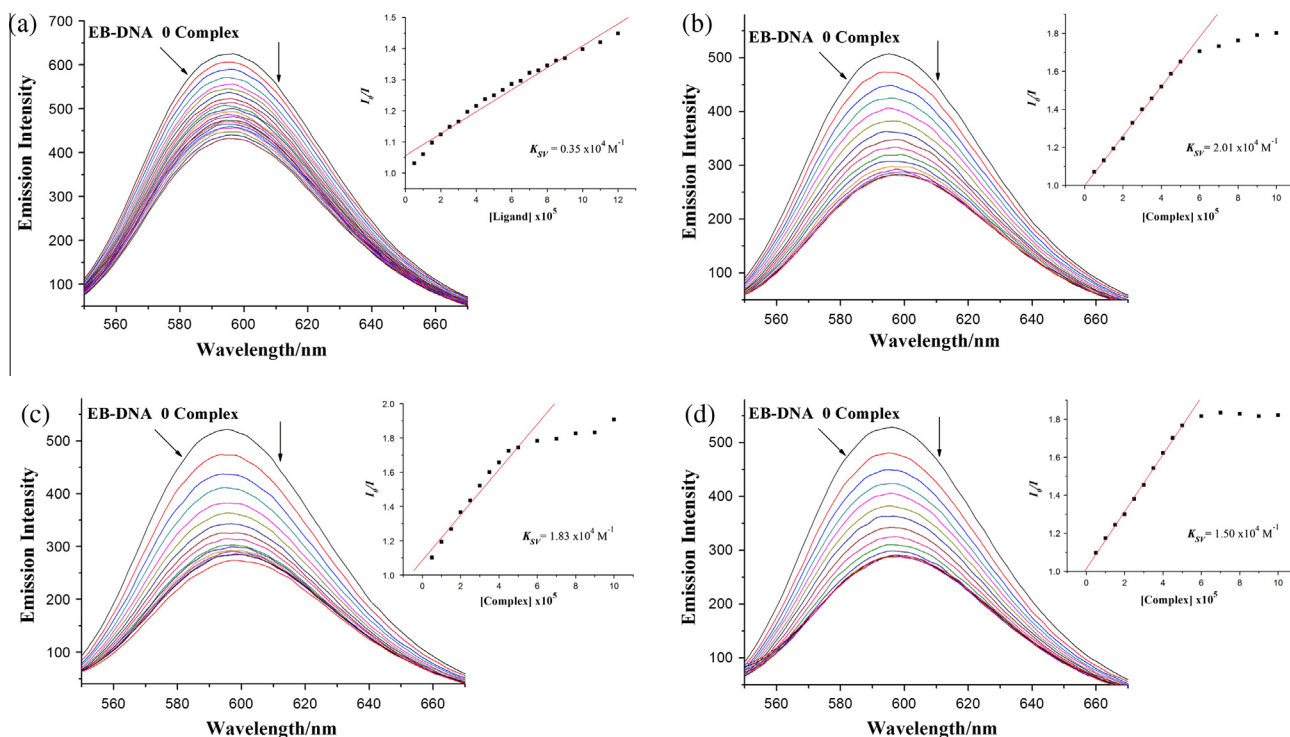


Fig. 8. Fluorescence spectra of the DMF solution of the ligand H_2L (a) and complexes **1** (b), **2** (c), and **3** (d) in Tris-HCl buffer upon addition of CT-DNA. [Complex] = $3 \times 10^{-5} \text{ M}$. Arrow shows the intensity changing upon increasing CT-DNA concentrations. A Stern–Volmer quenching plot of the Ln(III) complexes inserting in their own fluorescence spectra with increasing concentrations of CT-DNA.

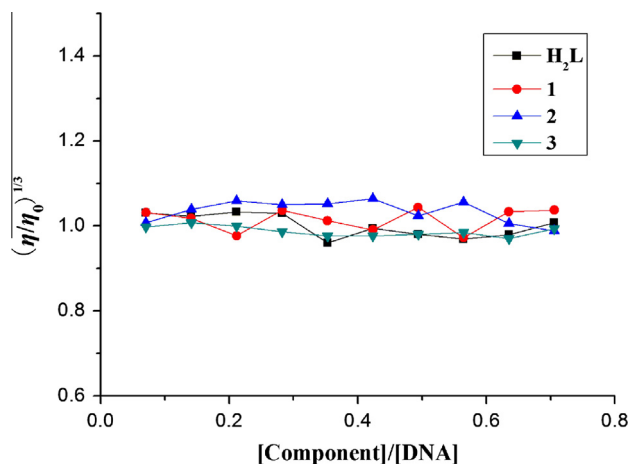


Fig. 9. Effect of increasing amounts of Ln(III) complexes on the relative viscosity of CT-DNA at 25.0 ± 0.1 °C.

radical-induced DNA damage in humans is at biologically relevant levels, with approximately 10^4 DNA bases being oxidatively modified per cell per day. Oxidative damage to DNA has been suggested to contribute to aging and various diseases including cancer and chronic inflammation [68]. Since among all reactive oxygen species, the hydroxyl radical ($\text{OH}\cdot$) and superoxide radical ($\text{O}_2^{\cdot-}$) are by far the most potent and therefore the most dangerous oxygen metabolite, elimination of these radicals is one of the major aims of antioxidant administration [69]. Consequently, in this paper, the ligand and its Ln(III) complexes (Ln = Sm, Eu and Tb) studied for their antioxidant activity by comparing their scavenging effects on hydroxyl radical ($\text{OH}\cdot$) and superoxide radical ($\text{O}_2^{\cdot-}$).

3.4.1. Hydroxyl radical scavenging activity

Fig. 10 shows the plots of hydroxyl radical scavenging effects (%) for the ligand and complexes 1–3. The values of IC_{50} of the ligand H_2L and complexes 1–3 for hydroxyl radical scavenging effects are $(7.13 \pm 0.102) \times 10^{-5}$ M, $(5.58 \pm 0.074) \times 10^{-5}$ M, $(3.39 \pm 0.091) \times 10^{-5}$ M and $(6.01 \pm 0.085) \times 10^{-5}$ M, respectively. The values of IC_{50} present the order $2 < 1 < 3 < \text{H}_2\text{L}$. It is proved that the hydroxyl radical scavenging effects of Ln(III) complexes are much higher than that of the ligand. Moreover, we compared the abilities of one present compounds to scavenge hydroxyl radical

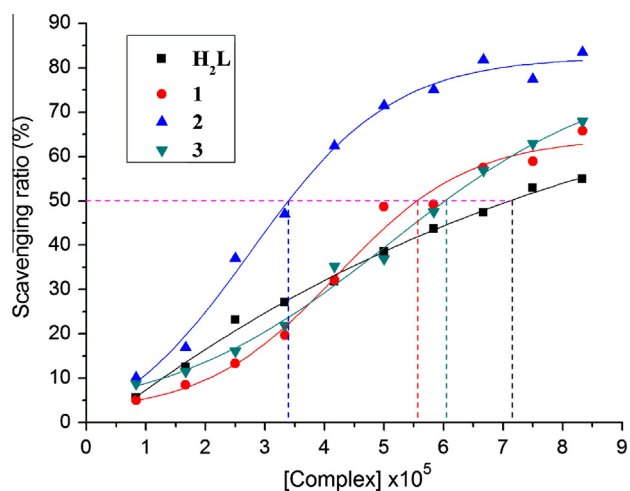


Fig. 10. The inhibitory effect of the ligand H_2L and three Ln(III) complexes on $\text{OH}\cdot$ radicals; the suppression ratio increases with increasing concentration of the test compound.

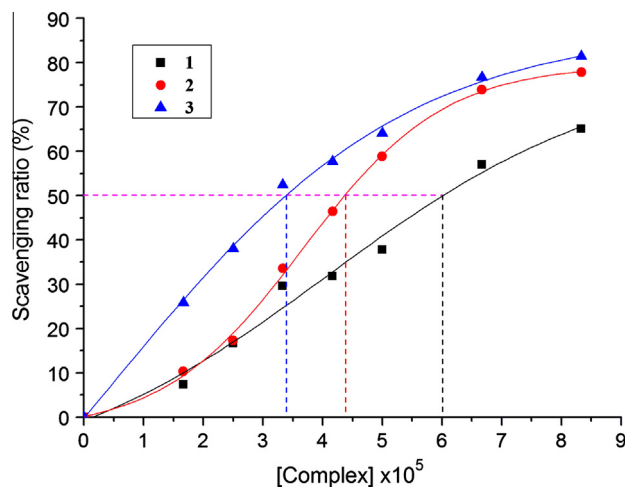


Fig. 11. The inhibitory effect of three Ln(III) complexes on $\text{O}_2^{\cdot-}$ radicals; the suppression ratio increases with increasing concentration of the test compound.

($\text{OH}\cdot$) with those of the well-known natural antioxidants mannitol and vitamin C, using the same method as reported in a previous paper [70]. The 50% inhibitory concentration (IC_{50}) value of mannitol and vitamin C are about 9.6×10^{-3} and 8.7×10^{-3} M, respectively. The results imply that the three Ln(III) complexes have the preferable ability to scavenge hydroxyl radical ($\text{OH}\cdot$) than mannitol and vitamin C. It can be concluded that a much less or no scavenging activity was exhibited by the ligand when compared to that of Ln(III) complexes which is due to the chelation of ligand with the central metal atom [69].

3.4.2. Superoxide radical scavenging activity

As another assay of antioxidant activity, superoxide radical ($\text{O}_2^{\cdot-}$) scavenging activity has been investigated. All the three Ln(III) complexes have good superoxide radical scavenging activity. As can be seen from Fig. 11, complexes 1–3 show the IC_{50} value of $(6.01 \pm 0.084) \times 10^{-5}$ M, $(4.38 \pm 0.065) \times 10^{-5}$ M and $(3.39 \pm 0.075) \times 10^{-5}$ M, respectively. The value of IC_{50} of vitamin C for superoxide radical scavenging effect is $(1.12 \pm 0.116) \times 10^{-4}$ M (Fig. S4). The values of IC_{50} present the order $3 < 2 < 1 < \text{vitamin C}$. The results imply that the three Ln(III) complexes (Ln = Sm, Eu and Tb) also have the preferable ability to scavenge superoxide radical ($\text{O}_2^{\cdot-}$) than vitamin C.

The lower IC_{50} values observed in hydroxyl radical and superoxide radical scavenging assays did demonstrate that the three Ln(III) complexes have some scavenging effects for hydroxyl radical ($\text{OH}\cdot$) and superoxide radical ($\text{O}_2^{\cdot-}$). However, due to the labile nature of aqueous lanthanide complexes and the toxicity of uncomplexed lanthanide ions, the Ln(III) complexes become an inhibitor (or a drug) to scavenge hydroxyl radical ($\text{OH}\cdot$) and superoxide radical ($\text{O}_2^{\cdot-}$) *in vivo* need further investigation.

4. Conclusion

In conclusion, the lanthanide (Sm(III), Eu(III) and Tb(III)) nitrate complexes of a pentadentate Schiff base ligand bis(*N*-salicylidene)-3-oxapentane-1,5-diamine (H_2L) have been synthesized and structurally characterized. The charge density and acidity of the lanthanide imposes evident influences on the coordination geometry leading to three different types of structure. The experimental results of DNA-binding about the Ln(III) complexes suggest that the ligand and Ln(III) complexes bind to DNA in a groove mode and the DNA-binding affinities of these three complexes follow the order $1 > 2 > 3$, which can be attributed to the electrostatics of positively charged Ln^{3+} ions and the charge transfer of coordinated

H₂L, caused by coordination of the central Ln(III). In addition, three Ln(III) complexes exhibited potential antioxidant activities against OH[•] and O^{2-•} radicals *in vitro* studies. These findings indicate that the Ln(III) complexes have many potential practical applications for the development of nucleic acid molecular probes and new therapeutic reagents for diseases on the molecular level. However, their pharmacodynamical, pharmacological and toxicological properties should be further studied *in vivo*.

Acknowledgements

The present research was supported by the National Natural Science Foundation of China (Grant No. 21367017), the Fundamental Research Funds for the Gansu Province Universities (212086), National Natural Science Foundation of Gansu Province (Grant No. 1212RJZA037), and 'Qing Lan' Talent Engineering Funds for Lanzhou Jiaotong University.

Appendix A. Supplementary material

Crystallographic data for complexes **1–3** have been deposited with the Cambridge Crystallographic Data Centre as supplementary publication CCDC reference numbers are 931951, 931952 and 931953, respectively. Copies of the data can be obtained, free of charge, on application to the CCDC, 12 Union Road, Cambridge CB2 1EZ, UK. Tel.: +44-01223-762910; fax: +44-01223-336033; e-mail: deposit@ccdc.cam.ac.uk or <http://www.ccdc.cam.ac.uk>. Supplementary data associated with this article can be found, in the online version, at <http://dx.doi.org/10.1016/j.jphotobiol.2014.04.005>.

References

- [1] V. Rajendiran, R. Karthik, M. Palaniandavar, H. Stoeckli-Evans, V.S. Periasamy, M.A. Akbarsha, B.S. Srinag, H. Krishnamurthy, Mixed-ligand copper(II)-phenolate complexes: effect of coligand on enhanced DNA and protein binding, DNA cleavage, and anticancer activity, *Inorg. Chem.* 46 (2007) 8208–8221.
- [2] P.T. Selvi, H. Stoeckli-Evans, M. Palaniandavar, Synthesis, structure and DNA interaction of cobalt(III) bis-complexes of 1,3-bis(2-pyridylimino)isoindoline and 1,4,7-triazacyclononane, *J. Inorg. Biochem.* 99 (2005) 2110–2118.
- [3] E.R. Jamieson, S.J. Lippard, Structure, recognition, and processing of cisplatin–DNA adducts, *Chem. Rev.* 99 (1999) 2467–2498.
- [4] S. Nafisi, M.A. Khalilzadeh, Z. Mokhtari, Interaction of β -carboline alkaloids with RNA, *DNA Cell Biol.* 29 (2010) 753–761.
- [5] S. Nafisi, M. Bonsai, P. Maali, F. Manouchehri, M.A. Khalilzadeh, F. Manouchehri, β -Carboline alkaloids bind DNA, *J. Photochem. Photobiol. B* 100 (2010) 84–91.
- [6] S. Roy, S. Saha, R. Majumdar, R.R. Dighe, A.R. Chakravarty, DNA photocleavage and anticancer activity of terpyridine copper(II) complexes having phenanthroline bases, *Polyhedron* 29 (2010) 2787–2794.
- [7] R.C. Todd, S.J. Lippard, Structure of duplex DNA containing the cisplatin 1,2-[Pt(NH₃)₂]²⁺-d(GpG) cross-link at 1.77 Å resolution, *J. Inorg. Biochem.* 104 (2010) 902–908.
- [8] O. Novakova, J. Malina, T. Suchankova, J. Kasparkova, T. Bugarcic, P.J. Sadler, V. Brabec, Energetics, conformation, and recognition of DNA duplexes modified by monodentate Ru^{II} complexes containing terphenyl arenes, *Chem. A Eur. J.* 16 (2010) 5744–5754.
- [9] H.L. Wu, J.K. Yuan, Y. Bai, G.L. Pan, H. Wang, J. Kong, X.Y. Fan, H.M. Liu, Synthesis, structure, DNA-binding properties and antioxidant activity of silver(I) complexes containing V-shaped bis-benzimidazole ligands, *Dalton Trans.* 41 (2012) 8829–8838.
- [10] H.L. Wu, J.K. Yuan, Y. Bai, G.L. Pan, H. Wang, X.B. Shu, Synthesis, structure, DNA-binding properties and antioxidant activity of a nickel(II) complex with bis(N-allylbenzimidazol-2-ylmethyl)benzylamine, *J. Photochem. Photobiol. B* 107 (2012) 65–72.
- [11] P. Kumar, B. Baidya, S.K. Chaturvedi, R.H. Khan, D. Manna, B. Mondal, DNA binding and nuclease activity of copper(II) complexes of tridentate ligands, *Inorg. Chim. Acta* 376 (2011) 264–270.
- [12] B.M. Zeglis, V.C. Pierre, J.K. Barton, Metallo-intercalators and metallo-insertors, *Chem. Commun.* 44 (2007) 4565–4579.
- [13] L.N. Ji, X.H. Zou, J.G. Liu, Shape- and enantioselective interaction of Ru(II)/Co(III) polypyridyl complexes with DNA, *Coord. Chem. Rev.* 216–217 (2001) 513–536.
- [14] F.N. Shi, L. Cunha-Silva, R.A.S. Ferreira, L. Mafra, T. Trindade, L.D. Carlos, F.A.A. Paz, J. Rocha, Interconvertible modular framework and layered lanthanide(III)-etidronic acid coordination polymers, *J. Am. Chem. Soc.* 130 (2008) 150–167.
- [15] B. Li, W. Gu, L.Z. Zhang, J. Qu, Z.P. Ma, X. Liu, D.Z. Liao, [Ln₂(C₂O₄)₂(pyzC)₂(H₂O)₂]_n [Ln = Pr (1), Er (2)]: novel two-dimensional lanthanide coordination polymers with 2-pyrazinecarboxylate and oxalate, *Inorg. Chem.* 45 (2006) 10425–10427.
- [16] Z. Chen, B. Zhao, Y. Zhang, W. Shi, P. Cheng, Construction and characterization of several new lanthanide–organic frameworks: from 2D lattice to 2D double-layer and to porous 3D net with interweaving triple-stranded helices, *Cryst. Growth Des.* 8 (2008) 2291–2298.
- [17] F.H. Li, G.H. Zhao, H.X. Wu, H. Lin, X.X. Wu, S.R. Zhu, H.K. Lin, Synthesis, characterization and biological activity of lanthanum(III) complexes containing 2-methylene-1,10-phenanthroline units bridged by aliphatic diamines, *J. Inorg. Biochem.* 100 (2006) 36–43.
- [18] H.X. Xu, H.Y. Zhang, X.G. Qu, Interactions of the human telomeric DNA with terbium–amino acid complexes, *J. Inorg. Biochem.* 100 (2006) 1646–1652.
- [19] M. Marinić, I. Piantanida, G. Rusak, M. Žinić, Interactions of quercetin and its lanthane complex with double stranded DNA/RNA and single stranded RNA: spectrophotometric sensing of poly G, *J. Inorg. Biochem.* 100 (2006) 288–298.
- [20] Z.Y. Yang, B.D. Wang, Y.H. Li, Study on DNA-binding properties and cytotoxicity in L₁₂₁₀ of La(III) complex with PMBP-isonicotinoyl hydrazone, *J. Organomet. Chem.* 691 (2006) 4159–4166.
- [21] B.D. Wang, Z.Y. Yang, T.R. Li, Synthesis, characterization, and DNA-binding properties of the Ln(III) complexes with 6-hydroxy chromone-3-carbaldehyde-(2'-hydroxy) benzoyl hydrazone, *Bioorgan. Med. Chem.* 14 (2006) 6012–6021.
- [22] W. Radecka-Paryzek, V. Patroniak, J. Lisowski, Metal complexes of polyaza and polyoxaaza Schiff base macrocycles, *Coord. Chem. Rev.* 249 (2005) 2156–2175.
- [23] P.A. Vigato, S. Tamburini, The challenge of cyclic and acyclic Schiff bases and related derivatives, *Coord. Chem. Rev.* 248 (2004) 1717–2128.
- [24] S. Liao, X.P. Yang, R.A. Jones, Self-assembly of luminescent hexanuclear lanthanide salen complexes, *Cryst. Growth Des.* 12 (2012) 970–974.
- [25] E. Gungor, H. Kara, Chiral one-dimensional hydrogen bonded, antiferromagnetic chloro-bridged dinuclear copper(II) complex with tridentate Schiff base ligand, *Inorg. Chim. Acta* 384 (2012) 137–142.
- [26] H.L. Wang, Z.Y. Yang, B.D. Wang, Synthesis, characterization and the antioxidative activity of copper(II), zinc(II) and nickel(II) complexes with naringenin, *Transit. Metal Chem.* 31 (2006) 470–474.
- [27] S.F. Lo, V. Mulabagal, C.L. Chen, C.L. Kuo, H.S. Tsay, Bioguided fractionation and isolation of free radical scavenging components from *in vitro* propagated chinese medicinal plants dendrobium tosaense makino and dendrobium moniliforme SW, *J. Agric. Food Chem.* 52 (2004) 6916–6919.
- [28] S.Y. Chiang, J. Welch, F.J. Rauscher, T.A. Beerman, Effects of minor groove binding drugs on the interaction of TATA box binding protein and TFIIA with DNA, *Biochemistry* 33 (1994) 7033–7040.
- [29] A.Y. Chen, C. Yu, B. Gatto, L.F. Liu, DNA minor groove-binding ligands: a different class of mammalian DNA topoisomerase I inhibitors, *Proc. Natl. Acad. Sci. USA* 90 (1993) 8131–8135.
- [30] S. Satyanarayana, J.C. Dabrowiak, J.B. Chaires, Tris(phenanthroline) ruthenium(II) enantiomer interactions with DNA: mode and specificity of binding, *Biochemistry* 32 (1993) 2573–2584.
- [31] M.F. Reichmann, S.A. Rice, C.A. Thomas, P. Doty, A further examination of the molecular weight and size of desoxyribose nucleic acid, *J. Am. Chem. Soc.* 76 (1954) 3047–3053.
- [32] S.M. Nalson, C.V. Knox, Diccopper(II) complexes of an N₆O₂ macrocycle and seven-co-ordinate manganese(II), iron(II), cobalt(II), nickel (II), copper(II), and zinc(II) complexes of its N₅O₂ open-chain precursor, *J. Chem. Soc. Dalton Trans.* 1983 (1983) 2525–2528.
- [33] Bruker, Smart Saint and Sadabs, Bruker Axis, Inc., Madison, WI, 2000.
- [34] G.M. Sheldrick, SHELXTL, Siemens Analytical X-ray Instruments Inc., Madison, Wisconsin, USA, 1996.
- [35] M.Q. Tian, H. Ihmels, S. Ye, Fluorimetric detection of Mg²⁺ and DNA with 9-(alkoxyphenyl)benzo[b]quinolinium derivatives, *Org. Biomol. Chem.* 10 (2012) 3010–3018.
- [36] D.S. Raja, N.S.P. Bhuvaneshb, K. Natarajan, A novel water soluble ligand bridged cobalt(II) coordination polymer of 2-oxo-1,2-dihydroquinoline-3-carbaldehyde (isonicotinic) hydrazone: evaluation of the DNA binding, protein interaction, radical scavenging and anticancer activity, *Dalton Trans.* 41 (2012) 4365–4377.
- [37] A. Wolf, G.H. Shimer, T. Meehan, Polycyclic aromatic hydrocarbons physically intercalate into duplex regions of denatured DNA, *Biochemistry* 26 (1987) 6392–6396.
- [38] A. Tarushi, G. Psomas, C.P. Raptopoulou, V. Psycharis, D.P. Kessissoglou, Structure and DNA-binding properties of bis(quinolonato)bis(pyridine)zinc(II) complexes, *Polyhedron* 28 (2009) 3272–3278.
- [39] J.R. Lakowicz, G. Webber, Quenching of fluorescence by oxygen probe for structural fluctuations in macromolecules, *Biochemistry* 12 (1973) 4161–4170.
- [40] C.P. Tan, J. Liu, L.M. Chen, S. Shi, L.N. Ji, Synthesis, structural characteristics, DNA binding properties and cytotoxicity studies of a series of Ru(III) complexes, *J. Inorg. Biochem.* 102 (2008) 1644–1653.
- [41] C.C. Winterbourn, Hydroxyl radical production in body fluids. Roles of metal ions, ascorbate and superoxide, *Biochem. J.* 198 (1981) 125–131.
- [42] Z.Y. Guo, R.E. Xing, S. Liu, H.H. Yu, P.B. Wang, C.P. Li, P.C. Li, The synthesis and antioxidant activity of the Schiff bases of chitosan and carboxymethyl chitosan, *Bioorg. Med. Chem. Lett.* 15 (2005) 4600–4603.

- [43] C. Beauchamp, I. Fridovich, Superoxide dismutase: improved assays and an assay applicable to acrylamide gels, *Anal. Biochem.* 44 (1971) 276–287.
- [44] Q.H. Luo, Q. Lu, A.B. Dai, L.G. Huang, A study on the structure and properties of a new model compound of Cu(II) Zn(II)-superoxide dismutase, *J. Inorg. Biochem.* 51 (1993) 655–662.
- [45] W.K. Dong, G. Wang, S.S. Gong, J.F. Tong, Y.X. Sun, X.H. Gao, Synthesis, structural characterization and substituent effects of two copper(II) complexes with benzaldehyde ortho-oxime ligands, *Transit. Metal Chem.* 37 (2012) 271–277.
- [46] H.L. Wu, F. Jia, F. Kou, B. Liu, J.K. Yuan, Y. Bai, A Schiff base N-(2-hydroxyacetophenone)-3-oxapentane-1,5-diamine and its copper(II) coordination polymer: synthesis, crystal structure, antioxidation, and DNA-binding properties, *J. Coord. Chem.* 64 (2011) 3454–3464.
- [47] K. Nakamoto, *Infrared and Raman Spectra of Inorganic and Coordination Compounds*, fourth ed., John Wiley & Sons, New York, 1986. p. 284.
- [48] L. Casella, M. Gullotti, A. Pintar, L. Messori, A. Rockenbauer, M. Győr, Iron(III) tyrosinate models. synthesis and spectroscopic and stereochemical studies of iron(III) complexes of *N*-salicylidene-*L*-amino acids, *Inorg. Chem.* 26 (1987) 1031–1038.
- [49] S.C. Manna, E. Zangrando, A. Bencini, C. Benelli, N.R. Chaudhuri, Syntheses, crystal structures, and magnetic properties of [Ln(III)₂(succinate)(3)(H₂O)(2)]center dot 0.5H₂O [Ln = Pr, Nd, Sm, Eu, Gd, and Dy] polymeric networks: unusual ferromagnetic coupling in Gd derivative, *Inorg. Chem.* 45 (2006) 9114–9122.
- [50] Y.P. Ren, L.S. Long, B.W. Mao, Y.Z. Yuan, R.B. Huang, L.S. Zheng, Nanoporous lanthanide-copper(II) coordination polymers: syntheses and crystal structures of [M₂(Cu₃(iminodiacetate)₆)]·8 H₂O]n (M = La, Nd, Eu), *Angew. Chem. Int. Edit.* 42 (2003) 532–535.
- [51] A. Biswas, M.G.B. Drew, C. Diaz, A. Bauzá, A. Frontera, A. Ghosh, *Cis-trans* isomerism in diphenoxido bridged dicopper complexes: role of crystallized water to stabilize the *cis* isomer, variation in magnetic properties and conversion of both into a trinuclear species, *Dalton Trans.* 41 (2012) 12200–12212.
- [52] E.M. Fatila, E.E. Hetherington, M. Jennings, A.J. Loughc, K.E. Preuss, Syntheses and crystal structures of anhydrous Ln(hfac)₃(monoglyme). Ln = La, Ce, Pr, Sm, Eu, Gd, Tb, Dy, Er, Tm, *Dalton Trans.* 41 (2012) 1352–1362.
- [53] M. Pietraszkiewicz, O. Pietraszkiewicz, J. Karpiuk, E. Karpiuk, T. Borowiak, G. Dutkiewicz, The first ternary europium tetraphenylimidodiphosphinate complex: X-ray structure and photoluminescent properties, *Inorg. Chim. Acta* 387 (2012) 426–430.
- [54] Y.C. Liu, Z.Y. Yang, Crystal structures, antioxidation and DNA binding properties of Dy(III) complexes with Schiff-base ligands derived from 8-hydroxyquinoline-2-carboxaldehyde and four aroylhydrazines, *Eur. J. Med. Chem.* 44 (2009) 5080–5089.
- [55] C. Behrens, N. Harrit, P.E. Nielsen, Synthesis of a Hoechst 32258 analogue amino acid building block for direct incorporation of a fluorescent, high-affinity DNA binding motif into peptides, *Bioconjugate Chem.* 12 (2001) 1021–1027.
- [56] V.G. Vaidyanathan, B.U. Nair, Photooxidation of DNA by a cobalt(II) tridentate complex, *J. Inorg. Biochem.* 94 (2003) 121–126.
- [57] R. Vijayalakshmi, M. Kanthimathi, V. Subramanian, B.U. Nair, Interaction of DNA with [Cr(Schiff base)(H₂O)₂]ClO₄, *BBA-Gen. Subjects* 1475 (2000) 157–162.
- [58] M.J. Waring, Complex formation between ethidium bromide and nucleic acids, *J. Mol. Biol.* 13 (1965) 269–282.
- [59] R. Gaura, R.A. Khanb, S. Tabassumb, P. Shahc, M.I. Siddiqic, L. Mishraa, Interaction of a ruthenium(II)-chalcone complex with double stranded DNA: spectroscopic, molecular docking and nuclease properties, *J. Photochem. Photobiol. A* 220 (2011) 145–152.
- [60] L.A. Bagatolli, S.C. Kivatinitz, G.D. Fidelio, Interaction of small ligands with human serum albumin IIIA subdomain. How to determine the affinity constant using an easy steady state fluorescent method, *J. Pharm. Sci.* 85 (1996) 1131–1132.
- [61] Q.H. Zhou, P. Yang, Synthesis, crystal structure and DNA binding studies of Zn(II) complex with 1,3-bis(benzimidazol-2-yl)-2-oxapropane, *Acta Chim. Sin.* 64 (2006) 793–798.
- [62] S.M. Nelson, L.R. Ferguson, W.A. Denny, Non-covalent ligand/DNA interactions: minor groove binding agents, *Mutat. Res.* 623 (2007) 24–40.
- [63] D.L. Boger, B.E. Fink, S.R. Brunette, W.C. Tse, M.P. Hedrick, A simple, high-resolution method for establishing DNA binding affinity and sequence selectivity, *J. Am. Chem. Soc.* 123 (2001) 5878–5891.
- [64] Z.Q. Liu, M. Jiang, Y.T. Li, Z.Y. Wu, J.X. Yang, One-dimensional copper(II) polymer with bridging μ -trans-oxamidate and thiocyanate ligands: synthesis, crystal structure and DNA binding studies, *Inorg. Chim. Acta* 362 (2009) 1253–1259.
- [65] D.S. Sigman, A. Mazumder, D.M. Perrin, Chemical nucleases, *Chem. Rev.* 93 (1993) 2295–2316.
- [66] R. Palchaudhuri, P.J. Hergenrother, DNA as a target for anticancer compounds: methods to determine the mode of binding and the mechanism of action, *Curr. Opin. Biotech.* 18 (2007) 497–503.
- [67] B.D. Wang, Z.Y. Yang, P. Crewdson, D.Q. Wang, Synthesis, crystal structure and DNA-binding studies of the Ln(III) complex with 6-hydroxychromone-3-carbaldehyde benzoyl hydrazine, *J. Inorg. Biochem.* 101 (2007) 1492–1504.
- [68] K. Tsai, T.G. Hsu, K.M. Hsu, H. Cheng, T.Y. Liu, C.F. Hsu, C.W. Kong, Oxidative DNA damage in human peripheral leukocytes induced by massive aerobic exercise, *Free Radical Bio. Med.* 31 (2001) 1465–1472.
- [69] N. Udilova, A.V. Kozlov, W. Bieberschulte, K. Frei, K. Ehrenberger, H. Nohl, The antioxidant activity of caroverine, *Biochem. Pharmacol.* 65 (2003) 59–65.
- [70] T.R. Li, Z.Y. Yang, B.D. Wang, D.D. Qin, Synthesis, characterization, antioxidant activity and DNA-binding studies of two rare earth(III) complexes with naringenin-2-hydroxy benzoyl hydrazone ligand, *Eur. J. Med. Chem.* 43 (2008) 1688–1695.